ACS OMEGA

Open Access

http://pubs.acs.org/journal/acsodf

Article

Optical Method for Detection and Classification of Heavy Metal Contaminants in Water Using Iso-pathlength Point Characterization

Alon Tzroya, Hamootal Duadi, and Dror Fixler*

Cite This: *ACS Omega* 2024, 9, 6986−6993

Read Online

ACCESS | Metrics & More | Article Recommendations

ABSTRACT: Water pollution caused by hazardous substances, particularly heavy metal (HM) ions, poses a threat to human health and the environment. Traditional methods for measuring HM in water are expensive and time-consuming and require extensive sample preparation. Therefore, developing robust, simple, and sensitive techniques for the detection and classification of HM is needed. We propose an optical approach that exploits the full scattering profile, meaning the angular intensity distribution, and utilizes the iso-pathlength (IPL) point. This point appears where the intensity is constant for different scattering coefficients, while the absorption coefficient is set. The absorption does not affect the IPL point position, it only reduces its intensity. In this paper, we explore the wavelength influence on the IPL point both in Monte Carlo simulations and experimentally. Next, we present the characterization of ferric chloride ($FeCl_2$) by this phenomenon. Eventually, we exhibit the detection of $FeCl_2$ and intralipid mixed in concentrations of 50−100 and 20−30 ppm, respectively. These findings endorse the idea that the IPL point is an intrinsic parameter of a system serving as an absolute calibration point. The method provides an efficient way of differentiating contamination in water. Its characterization technique is easy, precise, and versatile making it preferable for water monitoring.

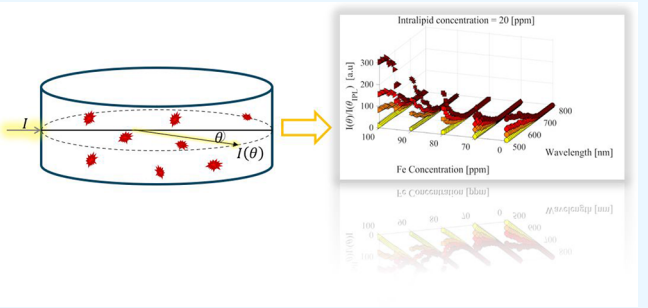

1. INTRODUCTION

Water pollution caused by anthropogenic activity and hazardous substance release has become a major concern, with heavy metal (HM) ions being a significant contributor due to their high toxicity and nondegradability.[1,2] Detecting HMs in drinking water can be done using two main strategies: spectroscopic and electrochemistry.[3] First, spectroscopic methods rely on the interaction of light with matter. Inductively coupled plasma mass spectrometry (ICP-MS) is a common, highly sensitive, and precise spectroscopic technique that can detect and quantify multiple HM ions simultaneously.[4] Another common spectroscopic technique is atomic absorption spectroscopy. This system involves the measurement of the absorption of light by metal ions at specific wavelengths and requires the medium in its gas state.[5] However, these systems are expensive, time-consuming, and require skilled operating personnel.[6,7] Other conventional optical methods are fiber grating, fluorescence sensing, optical absorbance, surface plasmon resonance, and Raman scattering.[6,8,9] Additionally, in some cases, using selective chromogenic reagents and indicator dyes is preferable.[10] The reagents and dyes react with a specific metal ion, enabling its detection. Nevertheless, such methods are complex to implement, including sensitivity and interference limitations, and require preprocessing for the samples.[3,6] Second, as opposed to spectroscopic methods, electrochemical methods are more cost-effective, user-friendly, and suitable for in-field applications.[11,12] The methods for reagents and dyes originated from measuring the electrical properties of solutions containing metal ions. For HM ion detection, there are amperometry, voltammetry, potentiometry, impedance measurement, and coulometry.[12] Among electrochemical procedures, anodic stripping voltammetry has been generally used for the analysis of HM ions.[11] However, electrochemical techniques are less sensitive and have a higher limit of detection compared to other procedures.[3] Also, these techniques require calibration and complex sample preparation.[12] As described above, various techniques are available for the detection of HM ions. There are also biosensing approaches such as fluorescent carbon dots and nanophotonic sensors with passive trapping of molecules.[13−15] However, a cost effective technique applicable to all metal ions that can detect HM in extremely low concentrations in real time is absent. Moreover, individually detecting and classifying HM in a single measurement is challenging since the

Received: November 5, 2023
Revised: January 13, 2024
Accepted: January 16, 2024
Published: February 5, 2024

metal ions may interfere with each other.[3] As a result, developing a sensitive method that allows for the real-time detection of a wide range of HMs is needed. Hence, we propose measuring the full scattering profile (FSP) and utilizing the iso-pathlength (IPL) point. Using this method in previous research enabled to accurately map and detect the contaminants type and concentrations in a single real-time measurement.[16] Our method's main advantage is its simple detection process. Initially, the FSP is measured, representing the angular intensity distribution of light from a cylindrical medium. The FSP is the intensity I, as a function of the angle θ, as seen in Figure 1.

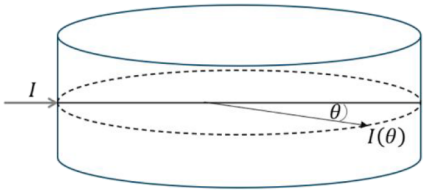

Figure 1. Light intensity (I) as a function of the angle (θ).

Then, the IPL point is used for calibration. This unique point lies on the sample surface where light intensity remains constant across a range of scattering coefficients (μ_s), which is the probability of a photon to experience a scattering event.[17] Similarly, the absorption coefficient (μ_a) is the probability of a photon to be absorbed in the material. Then, to determine the position of the point, several measurements of the samples using the FSP are needed, with the scattering coefficient being the only variable changed between each sample.[17,18] When the absorption coefficient is changed but the scattering is constant, the IPL point will not appear.[19] This implies that the IPL point grants the separation of scattering and absorption; changes in absorption do not affect the position of the IPL point, merely reducing its intensity.[16,19] Therefore, precisely determining the position of the IPL point involves careful sample preparation and keeping the absorption coefficient constant. Also, knowing the sample diameter is important because the IPL point position is proportional to the optical path length.[16,20] To address this, adjustments to the sample diameter or the distance between the detector and the sample can be made.[21] Hence, satisfying these conditions is important to ensure a consistent IPL point for each material. Previous research on the IPL point had been conducted on samples where light experiences multiple scattering events, known as the multiple scattering regime (the measured point is larger than $1/\mu_s'$ from the light source).[21−23] For the research of contaminants in drinking water, we study samples where light scatters only a few times, known as the single or intermediate scattering regime.[24] The scattering in the system is determined by the concentration of insoluble particles, their size, and the system's geometry.[25] Higher concentrations of insoluble particles result in more scattering events. To verify our scattering regime, we calculated the optical depth (OD), a parameter that differentiates between different scattering regimes and is described by

$$\mathrm{OD} = l\cdot(\mu_s + \mu_a) \quad (1)$$

where l is the geometric length.[24] In our work, intralipid (IL) and ferric chloride ($FeCl_2$) are used as contaminants. The concentrations of the contaminants are used to place the samples in the single-intermediate regime as OD < 3, which is in partial agreement with the referenced work.[24] Previously, the IPL point was observed in the single-intermediate scattering regime.[16] However, in this study, it is the first time that simulations of contaminated water within the single scattering regime exhibit this phenomenon with its wavelength dependency. In addition, we present the IPL point even for low concentrations of $FeCl_2$, which were utilized as the HM contaminant. The optical system employed for detecting contaminants in water is described. Afterward, we explain the sample preparation and simulation model employed. Next, we present the angular spectrum of the IL for different wavelengths both experimentally and theoretically. Then, we exhibit the detection of HM using the FSP and IPL points. Finally, we show that our analysis utilizes the IPL point phenomenon for the detection of IL and $FeCl_2$ in water.

2. MATERIALS AND METHODS

2.1. Optical Setup. The optical setup included a tungsten halogen (TH) white light source with 20 W power (HL-2000-HP-FHSA Light Source, Ocean Insight). The light source is collimated (F220SMA-532, Thorlabs) and illuminated the cylindrical sample of contaminated water. The FSP is measured using a collimated multicore optical fiber (M59L02−1000 μm-0.5NA, Thorlabs), which increases its active area to 50 mm^2. The optical fiber is placed on a rotating stage, allowing measurement at all angles. The detector is fixed at a constant distance of 3 mm from the sample surface, and it takes light intensity readings every 0.45°. The initial measurement position starts when the optical fiber and the light spot are collinear, at θ = 0°. To achieve reproducibility between measurements, we controlled the detector measurement angle (θ) using a stepper motor with a rotational accuracy of ±0.225°. The light spectrum is collected by a spectrometer, sent to MATLAB, and analyzed. The described system is shown in Figure 2.

2.2. Sample Preparation. The samples used in this study were composed of double-distilled water (ddw), contaminated with $FeCl_2$ and IL, a phospholipid-stabilized soybean oil (Sigma, 68890−65−3). The contamination concentration increased linearly between measurements with the incremental addition of each material. To examine the influence of the light

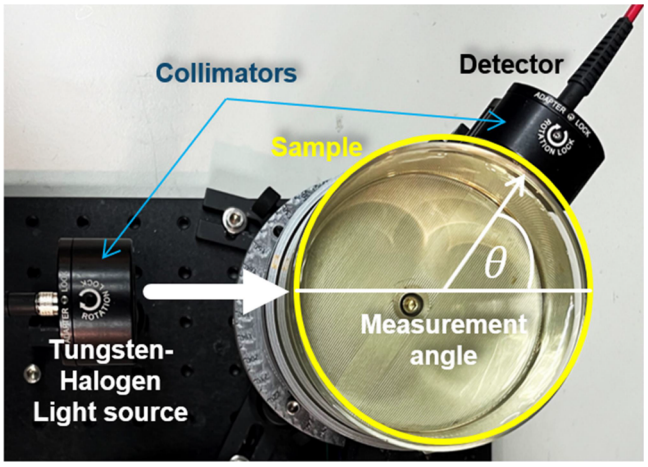

Figure 2. Optical setup in which a collimated TH white light source illuminates the cylindrical sample. A collimated multicore optical fiber is used to collect scattered light at different angles θ.

https://doi.org/10.1021/acsomega.3c08792
ACS Omega 2024, 9, 6986−6993

source wavelength on the IPL point within the single scattering regime, samples of contaminated water from the IL were utilized. The IL concentration was chosen to range between 20 and 40 ppm. The μ_s was evaluated using Mie approximation as follows.[26]

$$\mu_s = (2.54 \times 10^9)\cdot\lambda^{-2.4}\cdot c[\frac{1}{\text{cm}}] \quad (2)$$

where λ is the wavelength in nanometers and c is the sample concentration in ppm.

Hence, these concentrations were selected by evaluating their scattering coefficient and OD according to eqs 1 and 2 for 630 nm, the peak wavelength of the light source.[26] To explore the IPL phenomena in $FeCl_2$, we measured it in water with concentrations of 50−100 ppm in increments of 10 ppm. In addition, the absorption coefficient of $FeCl_2$ was verified by using a UV−vis spectrophotometer (Shimadzu, UV-1900, Japan). The absorption spectrum is presented in Figure 3 and was measured at a concentration of 1000 ppm. This high concentration was selected to get a good understanding of the spectrum.

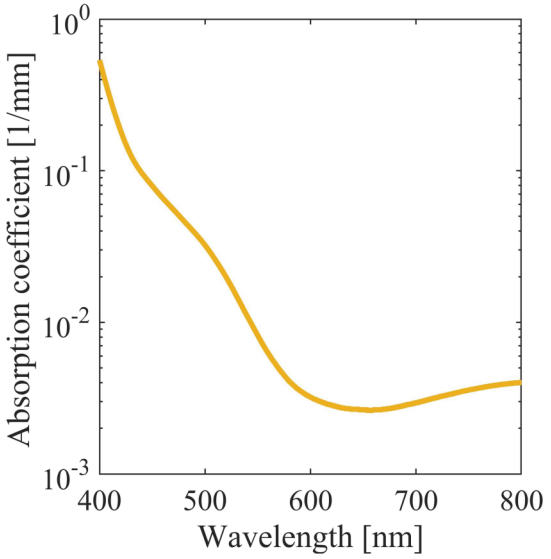

Figure 3. Absorption spectrum of $FeCl_2$ in a concentration of 1000 ppm.

Lastly, we measured IL and $FeCl_2$ when mixed in water. For this experiment, we verified that at 630 nm, where $FeCl_2$ absorption is minimal. The IPL point is at the same angle for both contaminants (IL and $FeCl_2$) based on the chosen concentrations. Hence, the contamination range for $FeCl_2$ and IL was from 50 to 100 and 20−30 ppm, respectively.

2.3. Simulations. For a theoretical understanding of the IPL point, we created a Monte Carlo (MC) simulation that describes the FSP. This method predicts the average behavior of a complex system by numerical calculations of random events.[27] We simulated the contaminated water with the IL and calculated the light propagation according to the experimental system mentioned in Figure 1. In the simulation, the photons deposit energy after every scattering event. Meaning, the probability of a photon to experience absorption is proportional to 1-albeado as seen in eq 3.

$$p(\text{absrob}) = 1 - \frac{\mu_s}{\mu_a + \mu_s} \quad (3)$$

The probability of a photon to scatter into a new trajectory is derived by Henyey−Greenstein phase function:[28]

$$p(\theta) = \frac{1}{2}\cdot\frac{1 - g^2}{1 + g^2 - 2g\cdot\cos(\phi)} \quad (4)$$

while g is the anisotropy of the material and ϕ is the scattering angle. The anisotropy of IL is evaluated using[26]

$$g = 1.1 - 0.58 \times 10^{-3}\cdot\lambda \quad (5)$$

Subsequently, we propagated photons according to MCML; we first generated z, a random scalar drawn from the uniform distribution in the interval (0,1). With it, we set the step size, s, by eq 6.

$$s = -\frac{\ln(z)}{\mu_a + \mu_s} \quad (6)$$

Thus, the photon is propagated in relation to the step size as shown in eq 6.

$$r_{\text{new}} = r_{\text{old}} + s\cdot k \quad (7)$$

where r is the position of the photon and k is the propagation vector of the photon acquired by ϕ. We repeat the calculations until the photon exits the cylindrical sample when its exit angle is saved. In this simulation, we present different scattering coefficients, which represent the contamination concentrations in water. Moreover, we counted the number of scattering events for each photon, confirming that merely 5% of the photons undergo more than 10 scattering events, aligning with the multiple scattering regime. From this, we deduced that the simulation effectively represents the single-intermediate scattering regime. So we chose to work with several μ_s values that are in the range of the single scattering regime to investigate the dependency of the IPL point on wavelength.

3. RESULTS

3.1. IPL Point Dependency on the Wavelength. The FSPs of water contaminated by IL were measured in the optical system (Figure 4) and simulated by the MC method (Figure 5). The experimental results are presented at 5° due to saturation in lower angles. Additionally, there is a small difference in the wavelengths due to the spectrometer and the initialization of the MC simulation. In each wavelength, the results exhibit the IPL point phenomenon (marked with a blue circle), where light intensity remains constant regardless of the scattering coefficient values. These findings emphasize that when the angles are below the IPL point, there is an inverse correlation between the scattering coefficient and the measured light intensity. In other words, prior to reaching the IPL point, a sample with a higher μ_s (as indicated by the yellow curves) leads to a lower intensity reading. However, when the angles exceed the IPL point, this trend is reversed with higher scattering coefficients resulting in higher light intensity readings. This characteristic of the IPL point has been observed in single wavelength measurements within the single and multiple scattering regimes before.[29] This is the first time that the dependency of the IPL point on wavelengths was simulated and measured using a broadband light source.

https://doi.org/10.1021/acsomega.3c08792
ACS Omega 2024, 9, 6986−6993

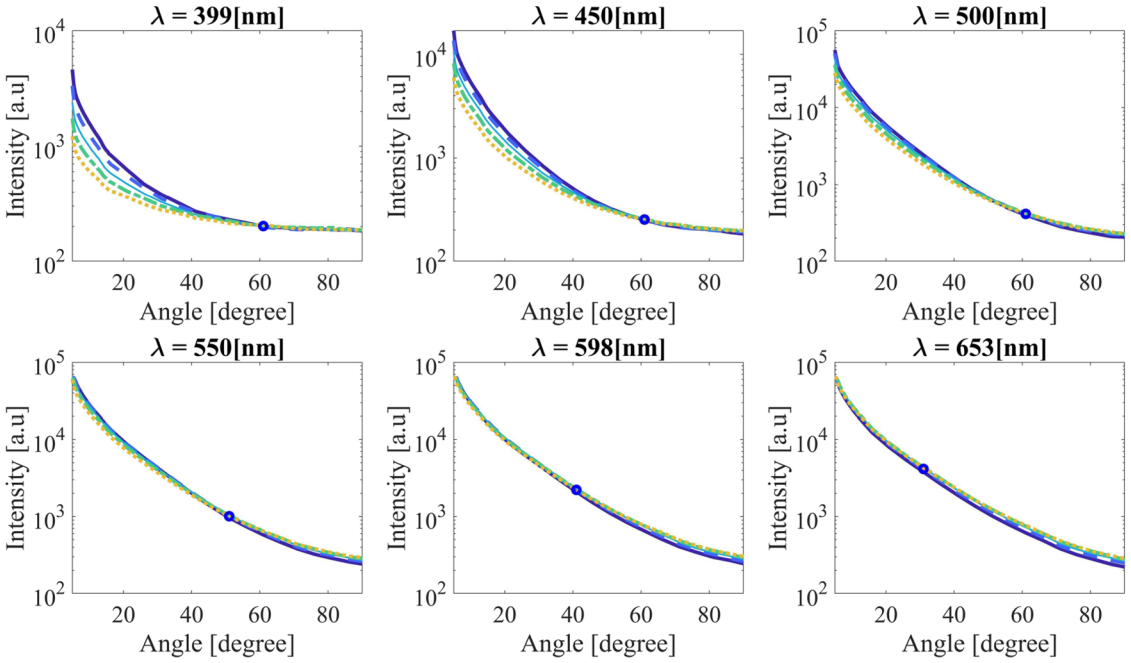

Figure 4. Experimental measurements of the FSP for IL samples ranging between 20 and 40 ppm in different wavelengths starting from 5°. The line style specifies the IL concentration ("wide solid blue line", "dashed light blue line", "slim solid cyan line", "dash-dotted green line", and "dotted yellow line" corresponding to 20, 25, 30, 35, and 40 ppm, respectively). The IPL point is marked by a blue circle.

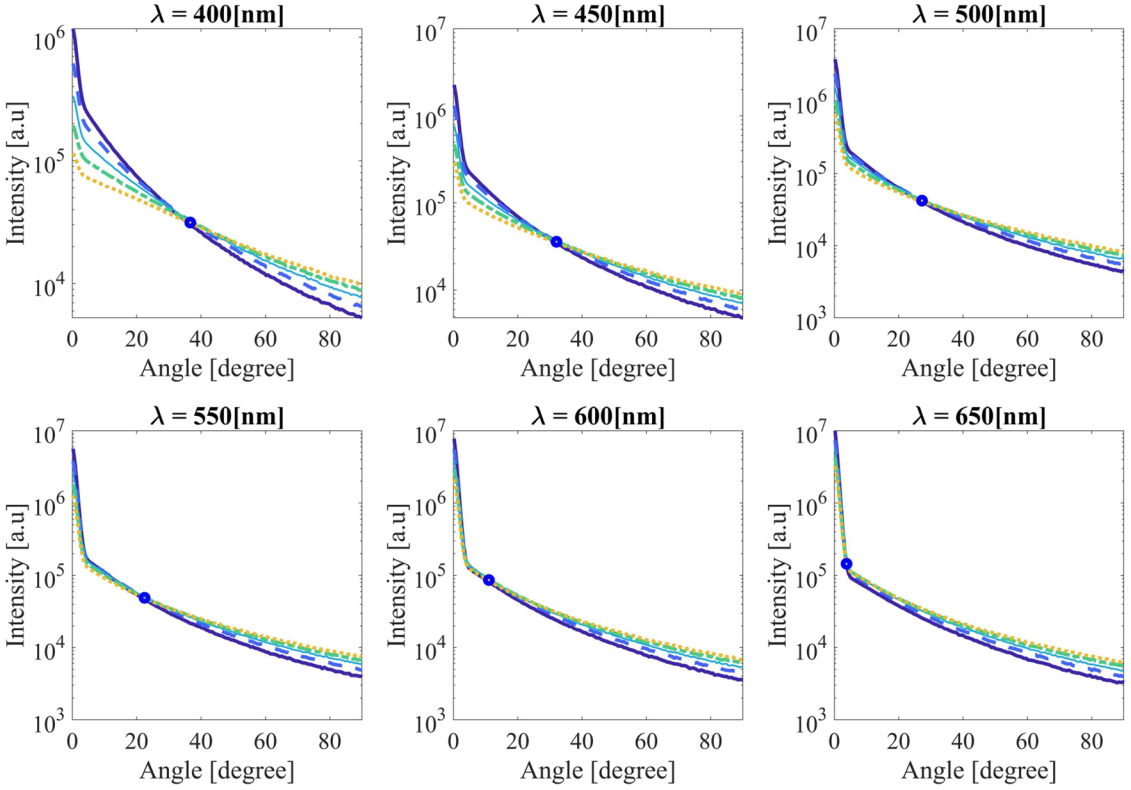

Figure 5. Simulation results of the FSP for a cylindrical sample of water contaminated by IL at concentrations of 20−40 ppm in different wavelengths. The line styles indicate the IL concentration ("wide solid blue line", "dashed light blue line", "slim solid cyan line", "dash-dotted green line", and "dotted yellow line" matching to 20, 25, 30, 35, and 40 ppm, respectively). The IPL points are marked by a blue circle.

In both the MC simulation and experiments, the IPL point was extracted for each wavelength within the range of 400−800 nm, enabling one to examine the dependency between the IPL point and wavelength, as depicted in Figure 6. It shows that the IPL point appears at higher angles for shorter wavelengths. Notably, this property of the IPL point is evident despite the Gaussian profile of the light spectrum emitted by the TH light source. This behavior can be attributed to the Mie theory approximation presented in eq 2, whereas for shorter wavelengths, the value of μ_s increases as the scattering

https://doi.org/10.1021/acsomega.3c08792
ACS Omega 2024, 9, 6986−6993

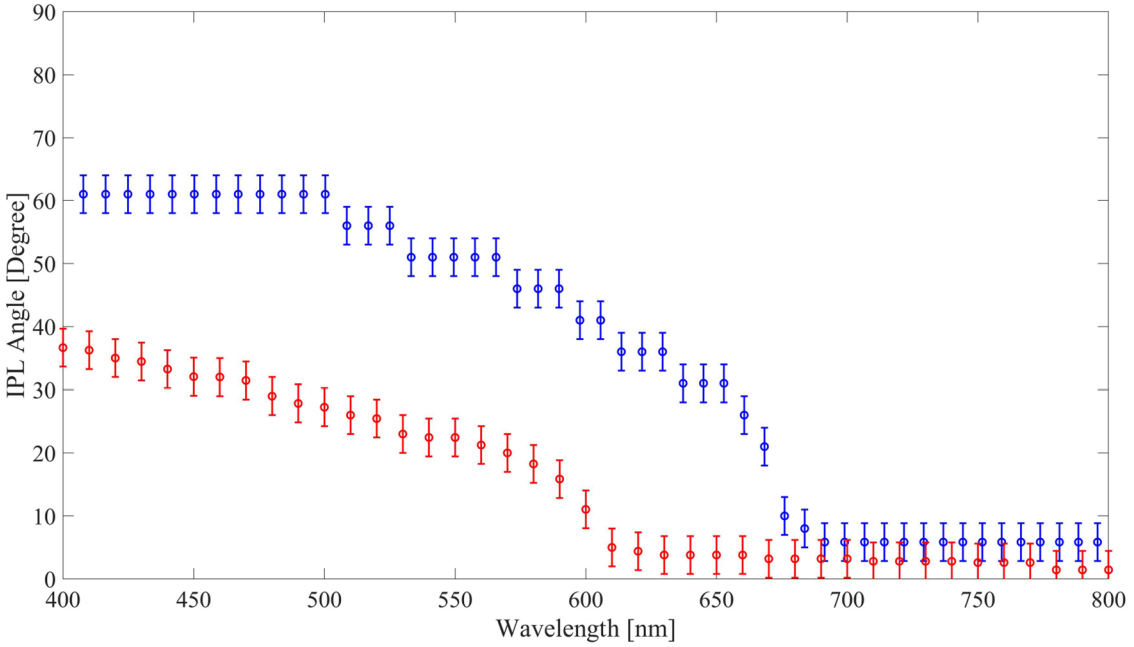

Figure 6. IPL point position of IL as a function of the wavelength extracted from simulations (red dots) and experiments (blue dots).

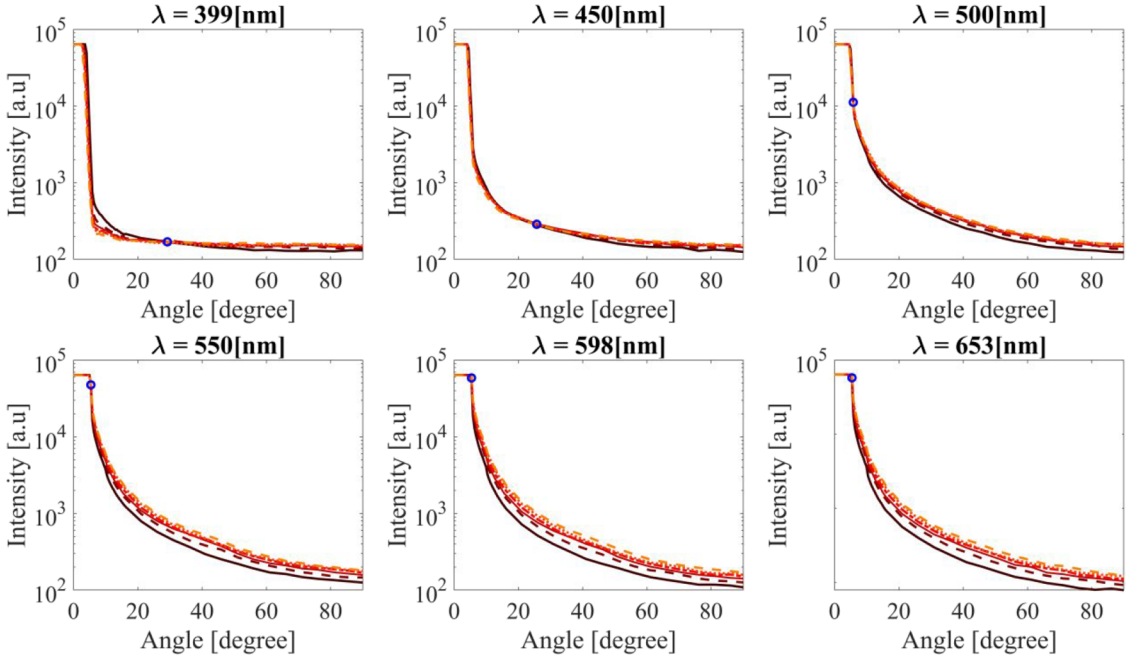

Figure 7. Measurements of the FSPs for ferric chloride ($FeCl_2$) samples in concentrations of 50−100 ppm in different wavelengths. The line style corresponds to the $FeCl_2$ concentration ("wide solid brown line", "dashed light brown line", "slim solid bourdeaux line", "dash-dotted red line", "dotted light red line and dashed orange line" matching to 50, 60, 70, 80,90 and 100 ppm, respectively). The crossing point is marked by a blue circle.

strengthens. This means that a higher wavelength does not have enough energy to strongly scatter the particles resulting in the appearance of the IPL point further form the source. This can be seen in the experiment from 680 nm and in the simulation from 610 nm. Note that due to the detector surface area, the accuracy of our system is 5°; hence, the experimental line may appear as a discontinuous function when compared to the simulation. Also, there are conditions in the experimental system that are different from the ideal simulation, resulting in a significant difference at short wavelengths.

3.2. FSP Measurements of $FeCl_2$. In this experiment, we measured the FSPs of water contaminated by $FeCl_2$ at different concentrations. The measured FSP results for selected wavelengths are presented in Figure 7, while the crossing point is marked by a blue circle. Identical to the IL seen in Figure 4, there is an inverse relationship between the scattering coefficient and the measured light intensity. This relationship is most clearly evident at 399 nm, where the curve representing the 50 ppm concentration exhibits higher intensity than others up to 38°. Beyond this point, the trend reverses, and the curve

https://doi.org/10.1021/acsomega.3c08792
ACS Omega 2024, 9, 6986−6993

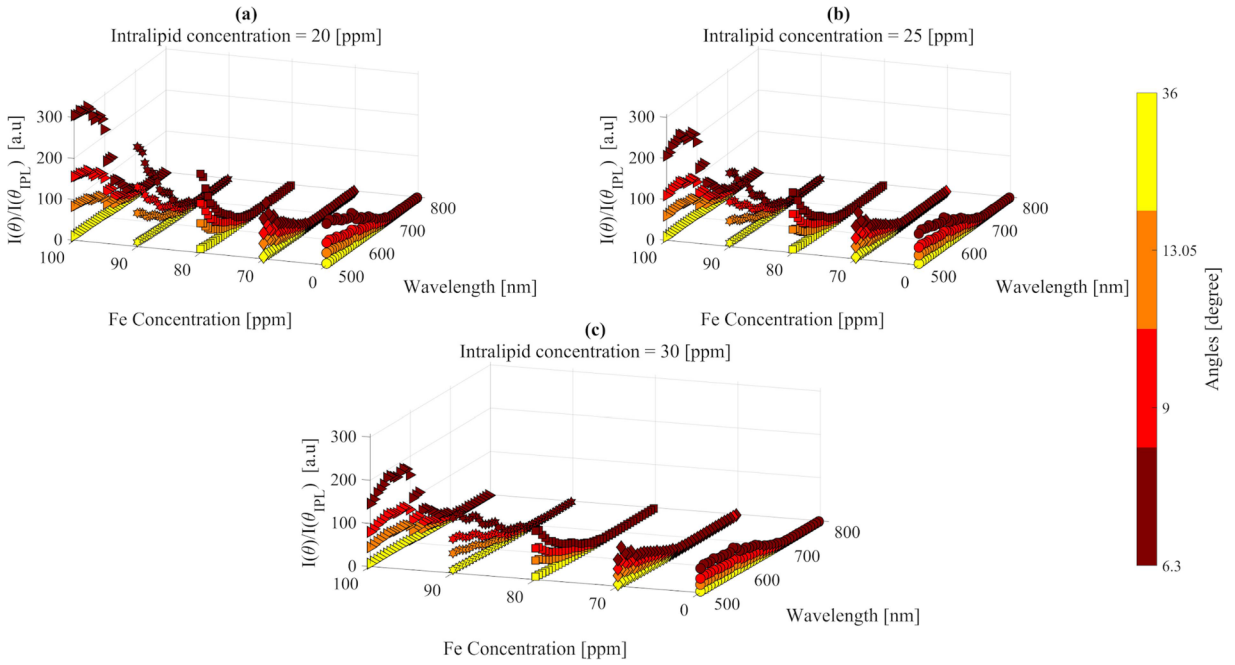

Figure 8. 3D analysis for the detection of $FeCl_2$ and IL. The colors represent different angles of measurement, corresponding to the color bar. The ticks match the $FeCl_2$ concentration ("circle", "diamond", "square", "asterisk", and "triangle" corresponding to 0, 70, 80, 90, and 100 ppm). The subplots (a), (b), and (c) represent IL concentrations of 20, 25, and 30 ppm, respectively.

displays the lowest intensity. Nevertheless, we must consider the fact that $FeCl_2$ is highly absorbing in lower wavelengths; thus, the point seen in the graph may not be the IPL point but rather an artificial point. Hence, we mainly see the IPL point in wavelengths higher than 500 nm.

3.3. Detecting HM and IL Using the IPL point. To distinguish between HM and IL, the measurement of the mixed samples was taken. The FSPs of the mixed samples were analyzed, and the IPL point was extracted. In a previous work, examining absorption and scattering individually revealed that scattering models the FSP, while absorption attenuates it.[19] By incorporating this theory, we proved the detection of IL and India ink by utilizing the IPL point.[16] However, since $FeCl_2$ both scatters and absorbs, a different approach is necessary. We focused on optimizing the utilization of the FSP and IPL points to detect and identify multiple materials across various wavelengths. Therefore, we created a 3D plot shown in Figure 8. Since $FeCl_2$ absorption at low wavelengths is not negligible, we analyze our results at wavelengths higher than 500 nm. In this plot, we represent the intensity in a measurement angle divided by the intensity in the IPL point as a function of wavelength and $FeCl_2$ concentration (also represented in different markers). The different colors represent different angles. Because our mixed samples also contain IL, we created this 3D analysis for each of the IL concentrations (Figure 8a−c represents an IL concentration of 20, 25, and 30 ppm, respectively). Analyzing Figure 8 revealed that as the Fe concentration increases, the spectrum rises in all angles and IL concentration. Additionally, the light spectrum shape is different from the IL compared to the mixed samples spectrum. For example, in Figure 8c, the shape of the spectrum in 100 ppm Fe is different than in 0 ppm. Moreover, the figure exhibits an attenuation of the spectrum as IL concentration increases (most clearly seen by comparing 100 ppm between Figure 8a−c). Thus, we exploited the spectra as a tool to detect the contaminants when mixed. Since different shapes of the spectrum represent different $FeCl_2$ concentrations, while their intensity correlates with the IL concentration.

This result can be elucidated by the decline in intensity readings in angles lower than the IPL when the IL concentration increases (as seen inSection 3.1). Similarly, yet not seen in this figure, this trend is flipped at angles higher than the IPL point.

In this presented data, there are outliers; these deviations may derive from the positioning of the sample in the optical setup or the lack of glass uniformity. One could think it may be rooted from the light source instability or from the spectrometer. However, since each sample is calibrated by the intensity in the IPL point, these deviations are not relevant, as the position of the IPL point depends solely on the geometry of the sample and the range of scattering.[16,19,22]

4. DISCUSSION AND CONCLUSIONS

In this study, we showed the correlation between the excitation wavelength and the IPL point angle both experimentally and in MC simulations while using IL as a scattering and contaminating substance. In addition, we exhibited the presence of the IPL point for HM in the single scattering regime using a definite range of $FeCl_2$ concentrations (50−100 ppm) in longer wavelength when the absorption can be neglected. This implies that the IPL point is evident as long as the substance scatters light, even in HM. These results indicate that regardless of the material, as the wavelength shortens the scattering strengthens, which results in a higher IPL point, as long as its absorption is insignificant. Consequently, we presented how we used this phenomenon to detect both IL and $FeCl_2$ while they were mixed in a series of samples. The spectrum shape indicates whether there is $FeCl_2$ and IL and the respective intensity points to the concentration. Moreover, this method is established as an enhanced method to detect contaminants in water and theoretically can detect multiple

https://doi.org/10.1021/acsomega.3c08792
ACS Omega 2024, 9, 6986−6993

contaminants, even more than two, in a single measurement. Given that our analysis method provides numerous parameters on the medium including the shape of the FSP, scattering at various angles, and sample absorption, we assume that leveraging them with further research will yield the detection of complementary materials in a single measurement. This means that using the enhanced method improves the differentiation of the optical properties between materials, enabling the identification of materials based on their spectral fingerprint. Furthermore, the information in Figure 3 supports our results in Section 3.2. As we can tell, the intensity across all angles is significantly lower for shorter wavelengths in contrast to higher wavelengths. Nevertheless, this implies that the IPL point is evident when μ_a is constant, and when analyzing the crossing point position seen in Figure 7, it converges at 5.4 ± 0.5° when λ is greater than 500 nm. This supports the data from Figure 3 where around 500 nm μ_a becomes negligible as it decreases in an order of magnitude relative to 400 nm. This means that the crossing point in a longer wavelength than 500 nm is the IPL point, which aligns with the absorption spectrum characteristics of the material. However, these findings require further research. Errors in the analysis can be attributed to errors in sample preparations and differences between individual water samples. Yet, these findings show the successful detection of two entirely different contaminants and their concentration in a real-time measurement using the IPL phenomenon. With further research, we could detect more materials and even utilize machine learning tools to enhance our detection capabilities.

AUTHOR INFORMATION

Corresponding Author

Dror Fixler − *The Faculty of Engineering and the Institute of Nanotechnology and Advanced Materials, Bar Ilan University, Ramat Gan 5290000, Israel;* orcid.org/0000-0003-0963-7908; Email: Dror.Fixler@biu.ac.il

Authors

Alon Tzroya − *The Faculty of Engineering and the Institute of Nanotechnology and Advanced Materials, Bar Ilan University, Ramat Gan 5290000, Israel*

Hamootal Duadi − *The Faculty of Engineering and the Institute of Nanotechnology and Advanced Materials, Bar Ilan University, Ramat Gan 5290000, Israel*

Complete contact information is available at: https://pubs.acs.org/10.1021/acsomega.3c08792

Author Contributions

The research conceptualization was formed by D.F. In addition, D.F. and H.D. were responsible for the research supervision methodology. The sample preparation as well as the experiments was done by A.T. The investigation, optical characterization of the samples, and data analysis were done by A.T. The final validation was done by A.T. and H.D. The writing of the first draft was done by A.T. while D.F. together with H.D was responsible for the review and editing for improving the paper.

Notes

The authors declare no competing financial interest.

ABBREVIATIONS

FSP, full scattering profile; IPL, iso-path length; OD, optical depth; ddw, double distilled water; IL, intralipid; HM, heavy metal.

REFERENCES

(1) Organization, W. H. *Guidelines for drinking-water quality: incorporating the first and second addenda*; World Health Organization: 2022.

(2) Organization, W. H. *Water quality and health-review of turbidity: information for regulators and water suppliers*; World Health Organization, 2017.

(3) Malik, L. A.; Bashir, A.; Qureashi, A.; Pandith, A. H. Detection and removal of heavy metal ions: a review. *Environmental Chemistry Letters* **2019**, *17*, 1495−1521.

(4) Wilschefski, S. C.; Baxter, M. R. Inductively coupled plasma mass spectrometry: introduction to analytical aspects. *Clinical Biochemist Reviews* **2019**, *40* (3), 115.

(5) Gouda, A. A.; El Sheikh, R.; Youssef, A. O.; Gouda, N.; Gamil, W.; Khadrajy, H. A. Preconcentration and separation of Cd (II), Co (II), Cu (II), Ni (II), and Pb (II) in environmental samples on cellulose nitrate membrane filter prior to their flame atomic absorption spectroscopy determinations. *International Journal of Environmental Analytical Chemistry* **2023**, *103* (2), 364−377.

(6) Zamora-Ledezma, C.; Negrete-Bolagay, D.; Figueroa, F.; Zamora-Ledezma, E.; Ni, M.; Alexis, F.; Guerrero, V. H. Heavy metal water pollution: A fresh look about hazards, novel and conventional remediation methods. *Environmental Technology & Innovation* **2021**, *22*, No. 101504.

(7) Fathalla, M.; Selvaganapathy, P. R. Colorimetric Detection of Heavy Metal Ions Using Superabsorptive Hydrogels and Evaporative Concentration for Water Quality Monitoring. *ACS ES&T Water* **2022**, *2* (4), 658−666.

(8) Shakya, A. K.; Singh, S. State of the art in fiber optics sensors for heavy metals detection. *Opt. Laser Technol.* **2022**, *153*, No. 108246.

(9) Guo, Z.; Chen, P.; Yosri, N.; Chen, Q.; Elseedi, H. R.; Zou, X.; Yang, H. Detection of heavy metals in food and agricultural products by surface-enhanced Raman spectroscopy. *Food Reviews International* **2023**, *39* (3), 1440−1461.

(10) Chen, Z.; Zhang, Z.; Qi, J.; You, J.; Ma, J.; Chen, L. Colorimetric detection of heavy metal ions with various chromogenic materials: Strategies and applications. *Journal of Hazardous Materials* **2023**, *441*, No. 129889.

(11) Meng, R.; Zhu, Q.; Long, T.; He, X.; Luo, Z.; Gu, R.; Wang, W.; Xiang, P. The innovative and accurate detection of heavy metals in foods: A critical review on electrochemical sensors. *Food Control* **2023**, *150*, No. 109743.

(12) Bansod, B.; Kumar, T.; Thakur, R.; Rana, S.; Singh, I. A review on various electrochemical techniques for heavy metal ions detection with different sensing platforms. *Biosens. Bioelectron.* **2017**, *94*, 443−455.

(13) Toropov, N.; Cabello, G.; Serrano, M. P.; Gutha, R. R.; Rafti, M.; Vollmer, F. Review of biosensing with whispering-gallery mode lasers. *Light: Sci. Appl.* **2021**, *10* (1), 42.

(14) Miao, X.; Yan, L.; Wu, Y.; Liu, P. Q. High-sensitivity nanophotonic sensors with passive trapping of analyte molecules in hot spots. *Light: Sci. Appl.* **2021**, *10* (1), S.

(15) Hu, J.; Sun, Y.; Geng, X.; Wang, J.; Guo, Y.; Qu, L.; Zhang, K.; Li, Z. High-fidelity carbon dots polarity probes: revealing the heterogeneity of lipids in oncology. *Light: Sci. Appl.* **2022**, *11* (1), 185.

(16) Tzroya, A.; Erblich, S.; Duadi, H.; Fixler, D. Detecting Contaminants in Water Based on Full Scattering Profiles within the Single Scattering Regime. *ACS Omega* **2023**, *8* (26), 23733−23738.

(17) Feder, I.; Duadi, H.; Fridman, M.; Dreifuss, T.; Fixler, D. Experimentally testing the role of blood vessels in the full scattering profile: solid phantom measurements. *J. Biomed. Photonics Eng.* **2016**, *2* (4), No. 040301, DOI: 10.18287/JBPE16.02.040301.

(18) Feder, I.; Wróbel, M.; Duadi, H.; Jędrzejewska-Szczerska, M.; Fixler, D. Experimental results of full scattering profile from finger tissue-like phantom. *Biomedical optics express* **2016**, *7* (11), 4695−4701.
(19) Feder, I.; Duadi, H.; Fixler, D. Single wavelength measurements of absorption coefficients based on iso-pathlength point. *Biomedical optics express* **2020**, *11* (10), 5760−5771.
(20) Duadi, H.; Feder, I.; Fixler, D. Linear dependency of full scattering profile isobaric point on tissue diameter. *Journal of biomedical optics* **2014**, *19* (2), No. 026007.
(21) Duadi, H.; Feder, I.; Fixler, D. Influence of detector size and positioning on near-infrared measurements and ISO-pathlength point of turbid materials. *Front. Phys.* **2021**, *9*, 43.
(22) Feder, I.; Duadi, H.; Chakraborty, R.; Fixler, D. Self-calibration phenomenon for near-infrared clinical measurements: theory, simulation, and experiments. *ACS omega* **2018**, *3* (3), 2837−2844.
(23) Feder, I.; Duadi, H.; Fixler, D. Effect of Spatial Modulated Light on Position of Self-Calibration Point. *IEEE Photonics Journal* **2021**, *13* (4), 1−5.
(24) Berrocal, E.; Sedarsky, D. L.; Paciaroni, M. E.; Meglinski, I. V.; Linne, M. A. Laser light scattering in turbid media Part I: Experimental and simulated results for the spatial intensity distribution. *Opt. Express* **2007**, *15* (17), 10649−10665.
(25) Hahn, D. W. *Light scattering theory*; Department of Mechanical and Aerospace Engineering; University of Florida, 2009.
(26) Van Staveren, H. J.; Moes, C. J.; van Marie, J.; Prahl, S. A.; Van Gemert, M. J. Light scattering in lntralipid-10% in the wavelength range of 400−1100 nm. *Applied optics* **1991**, *30* (31), 4507−4514.
(27) Wang, L.; Jacques, S. L.; Zheng, L. MCML—Monte Carlo modeling of light transport in multi-layered tissues. *Computer methods and programs in biomedicine* **1995**, *47* (2), 131−146.
(28) Henyey, L. G.; Greenstein, J. L. Diffuse radiation in the galaxy. *Astrophys. J.* **1941**, *93*, 70−83.
(29) Duadi, H.; Feder, I.; Fixler, D. Near-infrared human finger measurements based on self-calibration point: Simulation and in vivo experiments. *J. Biophotonics* **2018**, *11* (4), No. e201700208.

https://doi.org/10.1021/acsomega.3c08792
ACS Omega 2024, 9, 6986−6993